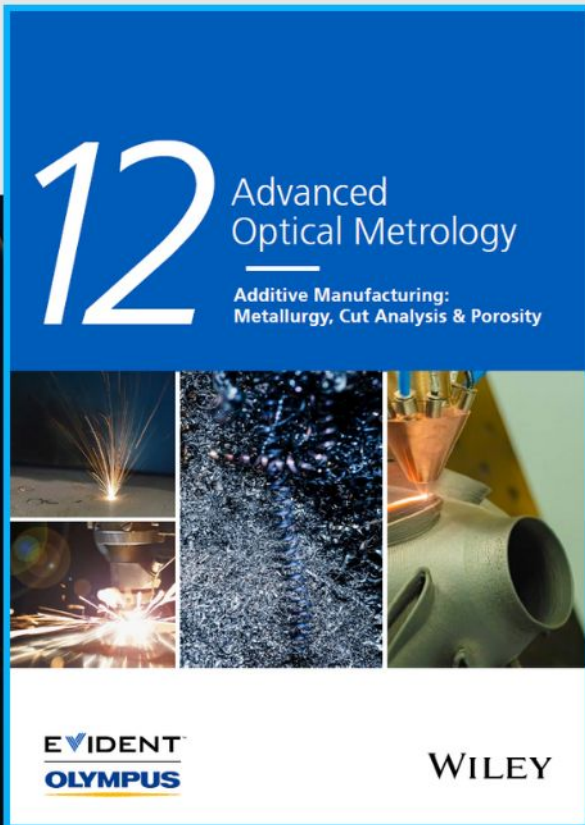# Additive Manufacturing: Metallurgy, Cut Analysis & Porosity

The latest eBook from Advanced Optical Metrology. Download for free.

In industry, sector after sector is moving away from conventional production methods to additive manufacturing, a technology that has been recommended for substantial research investment.

Download the latest eBook to read about the applications, trends, opportunities, and challenges around this process, and how it has been adapted to different industrial sectors.

EVIDENT OLYMPUS

WILEY

RESEARCH ARTICLE

Plasma polymers from oregano secondary metabolites: Antibacterial and biocompatible plant-based polymers

Jesus Romo-Rico[1,2] | Smriti Murali Krishna[2,3] | Jonathan Golledge[2,4,5] |
Andrew Hayles[6] | Krasimir Vasilev[6,7] | Mohan V. Jacob[1]

[1]Electronics Materials Lab, College of Science and Engineering, James Cook University, Townsville, Queensland, Australia

[2]College of Medicine and Dentistry, James Cook University, Townsville, Queensland, Australia

[3]Atherothrombosis and Vascular Biology, Baker Heart and Diabetes Institute, Melbourne, Australia

[4]Queensland Research Centre for Peripheral Vascular Disease, James Cook University, Townsville, Queensland, Australia

[5]Department of Vascular and Endovascular Surgery, Townsville University Hospital, Townsville, Queensland, Australia

[6]UNISA STEM, Mawson Lakes, South Australia, Australia

[7]College of Medicine and Public Health, Flinders University, Bedford Park, South Australia, Australia

Correspondence
Mohan V. Jacob, Electronics Materials Lab, College of Science and Engineering, James Cook University, Townsville, QLD 4811, Australia.
Email: mohan.jacob@jcu.edu.au

Abstract

Bacterial infection of chronic wounds is a major healthcare problem that affects the quality of life of millions of patients worldwide and leads to a substantial healthcare cost burden. This project focused on the manufacture of a potential wound healing agent. Plasma polymers from oregano secondary metabolites (PP-OSMs) were fabricated by radiofrequency plasma-enhanced chemical vapor deposition (RF-PECVD) in continuous and pulse plasma modes at room temperature. The surface, biocompatibility, and antibacterial properties of the PP-OSMs were investigated. Polymers fabricated by RF-PECVD retained the functional groups of OSMs, promoted human dermal fibroblast adhesion, inhibited *Staphylococcus aureus* attachment, and eliminated *Pseudomonas aeruginosa*. The PP-OSM coatings are potential candidates for use in medical applications where cell bio-compatibility and antibacterial properties are required.

Plasma polymers from Oregano secondary metabolites
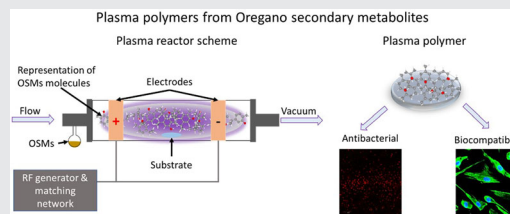
KEYWORDS

antibacterial, biocompatible, oregano, plant secondary metabolites, plasma polymers

1 | INTRODUCTION

Chronic wounds are a major issue that impacts the quality of life of 2% of the world's population[1] and places a huge burden on healthcare systems.[2–4] In Australia alone, chronic wound care costs more than AUD 3 billion per year and chronic wounds affect nearly half a million people.[5] Approximately, 50 000 Australians suffer from diabetic foot ulcers, whereas 300 000 are at risk of developing diabetic foot ulcers.[6] Diabetes-related chronic wounds frequently become infected, which impairs healing and can lead to major amputation and death.[7]

Plasma technology is being investigated as a novel method to fabricate wound healing materials such as plant secondary metabolites (PSMs), which have been reported to have antibacterial properties.[8–14] The antibacterial properties of PSMs are believed to result from incorporated monoterpenes inhibiting ATP generation, blocking ion transport, and disrupting cytoplasmic membranes of bacteria.[15–18]

One approach to coating PSMs on wound dressings is the use of radiofrequency plasma-enhanced chemical vapor deposition (RF-PECVD).[19] Plasma polymers (PP) from PSMs are formed by atoms, positive and negative ions, free and non-free radicals, and metastables, colliding in the plasma phase amongst themselves, intact precursor (PSMs), and the polymer coating. During this process, PSM molecules are partially or fully fragmented, reconstituted, and deposited on surfaces as highly crosslinked polymeric coatings.[20] The advantage of this technique is the capability to adjust the polymerization parameters to tune the final properties of the resulting polymeric surface. The RF-PECVD can be optimized to retain PSM functional groups in coatings deposited on different substrates to provide flexibility of application.

Previous studies have reported the use of terpinen-4-ol (T4), a major constituent of tea tree oil, as a PSM precursor to fabricate PP coatings.[21] Further, the antibacterial properties of T4 plasma films have been explored. Bazaka et al.[22] have fabricated antibacterial plasma films from T4 using a continuous plasma (CP) power of 10 and 25 W. The main difference between both polymers was the antibacterial response against *Staphylococcus aureus* and *Pseudomonas aeruginosa*. In the case of the polyterpenol films fabricated at 10 W, inhibition of bacterial adhesion was achieved by the preservation of functionalities of T4 during fabrication at low deposition power. Films fabricated at 25 W showed higher bacterial adhesion when compared to control and films fabricated at 10 W. This could be associated with the modification and recombination of T4 functional groups that promote bacterial adhesion instead of inhibition.[22]

In another study, Kumar et al.[23] developed coatings from T4 using plasma polymer (PP) polymerization. The polymerization conditions were 10 W and duty cycle (DC) 40 at 500 Hz. The antibacterial properties of these polymers were tested against *P. aeruginosa*. The polymers fabricated in this study were hydrophobic and promoted *P. aeruginosa* attachment; however, this pathogen was unable to survive after 24 h of contact with the T4 surface due to the retention of bactericidal molecules of the monomer.[23]

T4 polymers were fabricated and doped with ZnO nanoparticles using CP at 10 W, with and without oxygen (T4$_{oxy}$) and argon carriers (T4$_{arg}$). T4$_{oxy}$ and T4 + ZnO inhibited *Escherichia coli* adhesion. However, the antibacterial properties of the films did not change much with the addition of ZnO nanoparticles when compared to T4$_{oxy}$.[24] These results suggest that the contribution to bacterial inhibition is associated with the nature of T4 and the retention of its functional groups.

Pegalajar-Jurado et al.[25] fabricated films using a minor component of tea tree oil, 1,8-cineole, using plasma polymerization at 20 W. The obtained film was a moderate hydrophilic surface with roughness <1 nm. The antibacterial properties of the 1,8 cineole were retained in the PPs, showing inhibition of 64% against *S. aureus* and 98% against *E. coli* when compared to the control sample. A preliminary study on the biocompatibility of these films was also carried out. The 1,8 cineole films did not have cytotoxicity to fibroblasts and inhibited their adhesion to the polymeric matrix surface.[25]

Monomers of geranium essential oil were fabricated as continuous plasma films at a range of deposition power levels from 10 to 100 W.[26] The antibacterial properties of the created films reduced as the deposition power used increased, as a result of monomer fragmentation. At high deposition power, the functional groups defragment to a greater degree than at low power levels; thus, the inherent properties of the monomer are difficult to retain.

Oregano (*Origanum vulgaris*) is a popular herb widely used in Mediterranean and Latin American cuisines. Ancient civilizations not only used this herb to spice up their foods but also used it for treatment of respiratory infections, skin conditions, and digestive disorders. Oregano secondary metabolites (OSMs) are volatile molecules expelled by *Origanum vulgaris* that are believed to be responsible for the health benefits of oregano.[27–31] Antimicrobial activities of oregano have been attributed to its content of phenolic monoterpene carvacrol (CR). The different constituents of oregano oil can vary significantly. However, depending on the origin of the oregano species, the content of CR could be up to

approximately 90%.[32,33] CR affects bacterial membrane permeability, causing leakage of Na^+ and K^+, inhibition of intracellular enzyme activity, and irreparable damage in bacteria.[15]

Previous studies have examined the wound healing properties of oregano, but there has been no previous report of using RF-PECVD to fabricate OSMs.[34] The aim of this study was to fabricate PPs from OSMs with potential application as antibacterial surfaces for wound healing applications. We fabricated PP-OSMs using RF-PECVD in continuous and pulse modes. The retention of the functional groups of oregano in PP-OSMs was confirmed using Fourier transformed infrared spectroscopy (FTIR). Thickness, homogeneity, and hydrophilic properties were determined by ellipsometry, atomic force microscopy (AFM), and sessile drop water contact angle measurements, respectively. Leaching of the PP-OSM surface, as well as changes in the pH, were observed after submerging in water for 24 h. The antibacterial properties of the PP-OSMs were evaluated against *P. aeruginosa* and *S. aureus*. These bacteria were selected due to their high prevalence in diabetes-related wound infection.[35,36] Cell viability, cytotoxicity, and adhesion were evaluated in vitro using human dermal fibroblasts (HDFs).

2 | EXPERIMENTAL SECTION

2.1 | Fabrication of plasma films and chemical composition

PP-OSMs were fabricated on glass (76 mm × 26 mm) and borosilicate (diameter 6 mm) substrates. The substrates were sonicated for 5 minutes in propan-2-ol and then rinsed and sonicated with distilled water for 5 min. Afterward, the samples were air-dried. The substrates were introduced into an RF-PECVD plasma reactor, which consisted of a horizontally positioned tube chamber (*l*: 90 cm, *d*: 5 cm) with a rotary vacuum pump and a monomer inlet at each end. The rotary vacuum pump maintained the chamber at a pressure of 300 mTorr. Two copper electrodes were positioned at the middle of the tube chamber separated by 7 cm. During each experiment, the substrates were placed at the center between the electrodes. Both electrodes were coupled to a radiofrequency (RF) generator (ACG-3B; MKS Instrument). Two hundred microliters of Oregano essential oil (OEO) was placed in a Florence flask to feed the plasma reactor; the flow rate of the monomer was controlled with a vacuum stopcock. The deposition of the film was performed using CP and PP (DC of 50% and 500 Hz) modes at 50 W for 10 min.

2.2 | Chemical characterization

FTIR (Perkinelmer Inc.) was used to confirm the retention of Oregano functional groups in the PP-OSMs. For this purpose, FTIR was used in the attenuated total reflection (ATR) mode.

2.3 | Thickness and roughness

The thickness and topography of CP50W and PP50W were estimated using Variable Angle Spectroscopic Ellipsometry (JA Woollam-M200 D) at 55°, 60°, and 65°. Data acquisition parameters were standard and high accuracy modes. The 25 points of measurement were situated in a polar grid mesh starting from the center and forming the circle every 30°. A graded layer model (#slices = 5) consisting of a glass substrate layer and a B-spline were applied to the data within the 400–1000 nm region, where the film is optically transparent. Mean squared error lower than 1 was used in these analyses. The surface roughness of PP-OSMs was determined using an AFM (NT-MD) in the semicontact mode. The examination was carried out at room temperature, and the scanned area of the three-dimensional images was 9 μm^2. Three samples of each condition were measured; a minimum of three spots of 3 × 3 μm was analyzed.

2.4 | Wettability

Hydrophobic or hydrophilic properties in CP50W and PP50W could be determined from a contact angle test using a KSV CAM 101 optical apparatus. It has been reported that the wettability properties are related to the chemical composition and surface roughness of films.[37] Wettability represents the affinity of a liquid to spread on a surface, which is measured using contact angle analysis of PP-OSMs performed using the sessile drop method, where a drop of liquid (polar or disperse) is placed on the film surface and observed using a camera. The angle is measured using a reference baseline of the drop and the tangent of the drop boundary, the droplet volume, surface, and height, and the basal diameter.

2.5 | Bacterial studies

S. aureus (ATCC 25923) and *P. aeruginosa* (clinical isolate, PAO1 type; SA Pathology) were both retrieved from glycerol stocks stored at −80°C, plated onto tryptone soy agar plates, and cultured overnight at 37°C. For each strain, a single colony was aseptically

transferred to 2 ml of tryptone soy broth and incubated for 18 h. Triplicate samples of various essential oils plasma-coated onto fragmented glass slides were individually placed in six-well tissue culture plates and UV-sterilized for 20 min. Bare glass slides were UV-sterilized and used as the no-treatment control. Cell densities of the overnight cultures were measured using absorbance (600 nm, OD600) in a cuvette reader. The OD600 was set to 1, which is approximately 10^9 CFU/ml as previously determined by colony enumeration calibration. The cell density of the overnight cultures was then further diluted down to an approximate 10^6 CFU/ml. The glass slide samples were then immersed in 2 ml of the diluted cell cultures and incubated at 37°C for 18 h.

2.6 | LIVE/DEAD analyses

After incubation, the culture media were aspirated out of the well plates and replaced with 2 ml of phosphate-buffered saline (PBS) for 1 min to gently rinse away planktonic cells. The PBS was replaced, and the sample surfaces were coated with BacLight LIVE/DEAD (Invitrogen, Thermo Fisher Scientific) reagent, using equal proportions of Syto9 and propidium iodide at 1.5 µl/ml PBS. The samples were incubated for 15 min in the dark and immediately imaged using an Olympus FV3000 confocal laser scanning microscope. Three micrographs were taken at ×40 magnification at random locations on each replicate sample. Green- and red-stained cells were quantified using ImageJ software (V1.53; NIH).

2.7 | Fibroblast studies

HDF cells were cultured using the Fibroblast Growth Medium—2 Bullet kit—from Lonza™. Each experiment was conducted using cultured fibroblasts in passages 7 or 8. HDFs were seeded (~50 000 cells/ml) in 6 mm round borosilicate coverslips containing CP50W and PP50W using 100 µl of cell culture in 96-well plates. Lysed cells were used as a negative control, and healthy cells seeded on bare coverslips were used as a positive control.

2.8 | Cell viability and cytotoxicity

The ViaLight™ plus kit was used to estimate HDF viability by determining their ATP levels using the assay protocol for a 96-well plate published by Lonza. Toxi-light™ 100% lysis reagent set was used for determining cytotoxicity. This assay measures the release of adenylate kinase (AK) from damaged cells. AK actively phosphorylates ADP to form ATP, which is then measured in a luminometer POLAR STAR OMEGA Model 415-0530.

2.9 | Cell adhesion and spreading

HDFs with a density of 50 000 cells/ml were seeded on 16 mm round borosilicate substrates. After being cultured for 24 h, the cells were rinsed with PBS three times for 5 min and fixed with methanol at −20°C and rinsed again three times for 5 min with PBS. Subsequently, the primary antibody, vimentin (ab92547; Abcam), was added at a concentration of 1/200 for 1 h. or overnight at 4°C. The secondary antibody was then added, at a dilution factor of 1/500 or 1/1000 for 1 h. at room temperature. Finally, cell nuclei were counterstained with a drop of 4′,6-diamidino-2-phenylindole (DAPI) antifade gold (Thermo Fisher Scientific). Fluorescence images of cell nuclei and vimentin were observed using a fluorescence microscope Axio Imager Z1.

2.10 | Statistical analyses

In bacterial experiments, three biological replicates and three technical replicate images were obtained. Technical replicates were averaged, and the values were used to calculate the overall mean and standard deviation of cell viability across the three biological replicates. Data were plotted in GraphPad Prism (v8.3.0). Significance was determined with Prism, using a two-way analysis of variance (ANOVA) with Dunnett's multiple-comparisons test. In cell viability and cytotoxicity experiments, five replicates were performed. The mean and standard deviation were reported for each sample. Data were plotted using the same software. Significance was calculated using ANOVA multi-analyses comparison test.
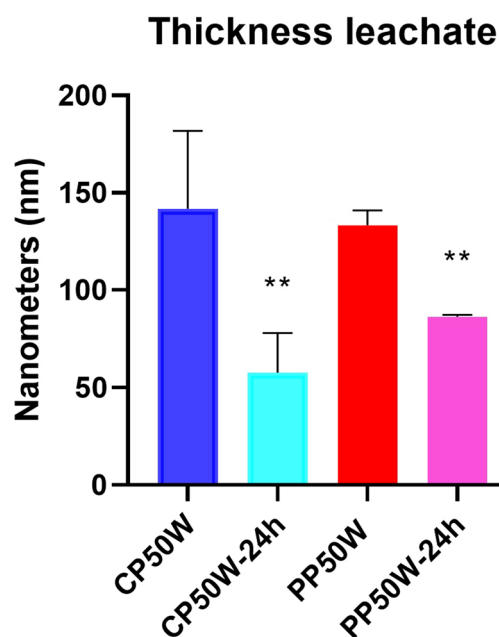
3 | RESULTS AND DISCUSSION

3.1 | Surface leachate as a pH modifier

The thicknesses of PP-OSMs, CP50W, and PP50W coatings were measured by Ellipsometry immediately after fabrication and after 24 h of immersion in MiliQ water (pH of 6.75). The average thicknesses of CP50W and PP50W films after fabrication were 90 and 123 nm, respectively. After immersion in water, CP50W lost 59.2% of the film thickness, whereas PP50W lost 35.3% of the film thickness as shown in Figure 1.

The pH of distilled water changed after 24 h due to the PP-OSM leachate from near-neutral pH of 6.75 to acidic pH of 4.6 and 5 for CP50W and PP50W, respectively. This result is interesting for wound dressing applications. In chronic wounds, elevated protease levels have been implicated in the degradation of new extracellular matrix (ECM). Protease activity is dependent on the pH of the surroundings.[38] One strategy for healing chronic wounds is to decrease protease levels using a pH modulator. The pH values of chronic wounds are in the range of 6.5–8.5; however, if this is reduced to 5, protease activity is expected to be reduced. Therefore, degradation of the new ECM would potentially not occur and wound healing might be promoted.[39]

Figure 2 shows the AFM images of CP50W and PP50W. Super smooth roughness, less than 1 nm, was obtained in both samples ($n = 3$) (CP50W = 0.2 nm and PP50W = 0.62 nm). The AFM image of PP50W showed random rough peaks (height = 1 nm) along the scanned area, whereas the image of CP50W showed a smooth surface. The observed 1 nm peaks along the PP50W
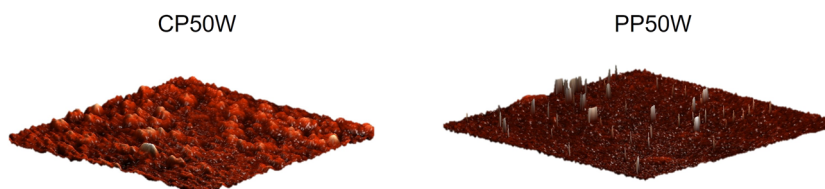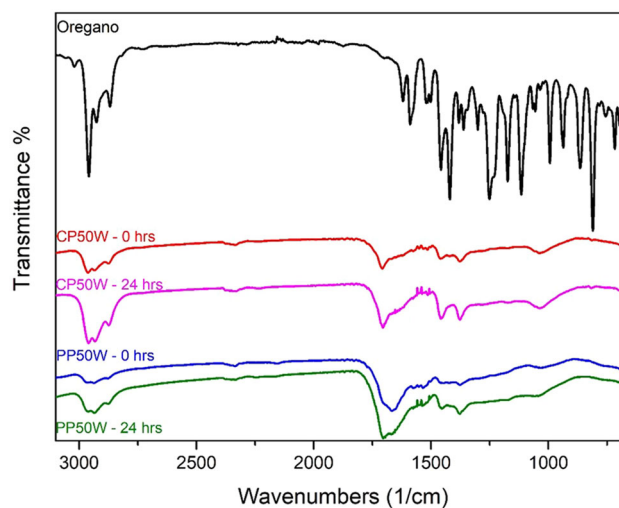
image could be related to the accumulation of large OSM molecules bound to its surface. Figure S2 shows the topography of both samples. The roughness of the PP-OSMs increased to around 10 nm in peaks and valleys after 24 h of submersion in MiliQ; this was associated with the leaching of thickness illustrated in Figure 1.

3.2 | Chemistry, wettability, and smoothness of PP-OSMs surfaces

The chemical properties of PP-OSMs were investigated by FTIR. Figure 3 shows the IR spectra of the PP-OSMs before and after they were submerged in MiliQ water. The functional groups of the OSMs were retained during PP-OSM fabrication and after 24 h of water submersion. The peaks between 2960 and 2866 cm^{-1} appear due to the vibration of the CH alkane strength and the CH$_2$ symmetric stretch. These peaks could be associated with the presence of CR.[40] At 1700 cm^{-1}, a peak in the spectra of both CP50W and PP50W images can be seen. This was likely due to the carboxyl COOH bonds formed due to the recombination of monomer molecules. Peaks between 1457 and 1380 cm^{-1} correspond to the symmetrical vibration of CH$_3$.[41–43] During continuous wave

FIGURE 1 Thickness of plasma polymer-oregano secondary metabolites (PP-OSMs) before and after being submerged in distilled water for 24 h

FIGURE 3 Fourier transform infrared spectrum of oregano essential oil, and plasma polymer-oregano secondary metabolites fabricated under different plasma conditions CP50W and PP50W

FIGURE 2 Surface images of CP50W and PP50W obtained by atomic force microscopy. The dimensions of the images are $3\,\mu m \times 3\,\mu m \times 3\,nm$

plasma deposition, the constant power leads to increasing fragmentation of the monomer and loss of some monomer functional groups, whereas pulsed-wave plasma deposition results in less fragmentation and retention of the monomer functional groups.[23] Therefore, the difference in the thickness between CP50W and PP50W could be related to the deposition time as well as the fragmentation effect of a plasma wave in the monomer and its polymerization.

The wettability of CP50W and PP50W was determined by water contact angle (WCA) measurements. The wettability of a material surface is related to its chemical composition and surface roughness.[37] Figure 4 shows the WCAs for the control, CP50W, and PP50W. The WCA for the control and CP50W was similar at around 45°. A WCA below 90° is considered hydrophilic, whereas a contact angle above 90° is considered hydrophobic. The WCA of PP50W was below 7°, which is considered superhydrophilic.[44] The low contact angle is likely associated with the high oxygen content observed in the FTIR measurements described above. COOH groups are polar groups that promote the absorption of water molecules on the surface.

3.3 | Antibacterial performance of oregano polymers

The antibacterial properties of CP50W and PP50W were evaluated by fluorescence imaging using a LIVE/DEAD bacterial viability kit. Using this kit, bacterial cells with an intact cell membrane fluoresce green, and cells with a perforated or ruptured cell membrane fluoresce red. Survival and attachment of *P. aeruginosa* and *S. aureus* were evaluated by the quantification of fluorescent cells. Figure 5a shows fluorescence images and Figure 5b shows viability and attachment plots of both microorganisms seeded in PP-OSMs and in a glass substrate used as a control.

Bactericidal activities of CP50W and PP50W are statistically significant (****$p < 0.0001$) against *P. aeruginosa*, with viabilities ranging from <1% (PP50W) up to 47% (CP50W), when compared to the glass slide control. However, as shown in Figure 5c, the rate of attachment of *P. aeruginosa* to CP50W and PP50W was not significantly different from the control.

CP50W and PP50W were effective against *S. aureus* viability, ***$p < 0.0005$ and *$p < 0.05$ respectively. Interestingly, *S. aureus* attachment was inhibited by both polymers, **$p < 0.005$ for PP50W and *$p < 0.05$ for CP50W. This suggests that the CP50W and PP50W plasma films have selective antifouling properties against *S. aureus*. The mechanisms of action of OEO, CR, and thymol (TH) against different pathogens have been elucidated. OEO, CR, and TH can kill *P. aeruginosa* and *S. aureus* by penetrating their cytoplasmic membrane, causing K^+ and PO_4^- leakages from both pathogens.[17] Recent studies of OEO against methicillin-resistant *S. aureus* reported that OEO destroys its cell membrane, causing irreversible damage and producing the leakage of Na^+ and K^+, thereby affecting its physiological function. Additionally, CR can form a chimera with bacterial DNA, affecting its replication, transcription, and translation.[15]

3.4 | Biocompatibility assessment: cell adhesion, viability, and cytotoxicity

Cell viability and cytotoxicity of fibroblasts were measured 24 h after seeding 0.1 ml of healthy cell medium (density 50 000 cells/ml) in a glass substrate (control), CP50W, and PP50W. After 24 h, cell viability in the control, CP50W, and PP50W was similar. However, CP50W and PP50W were less cytotoxic than the control, *$p < 0.05$ and **$p < 0.005$, respectively (Figure 6a). After 24 h of seeding, adhesion of cells was confirmed by
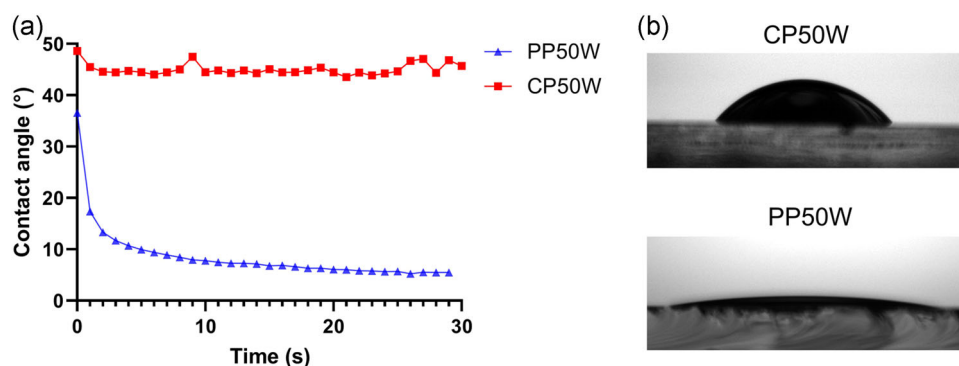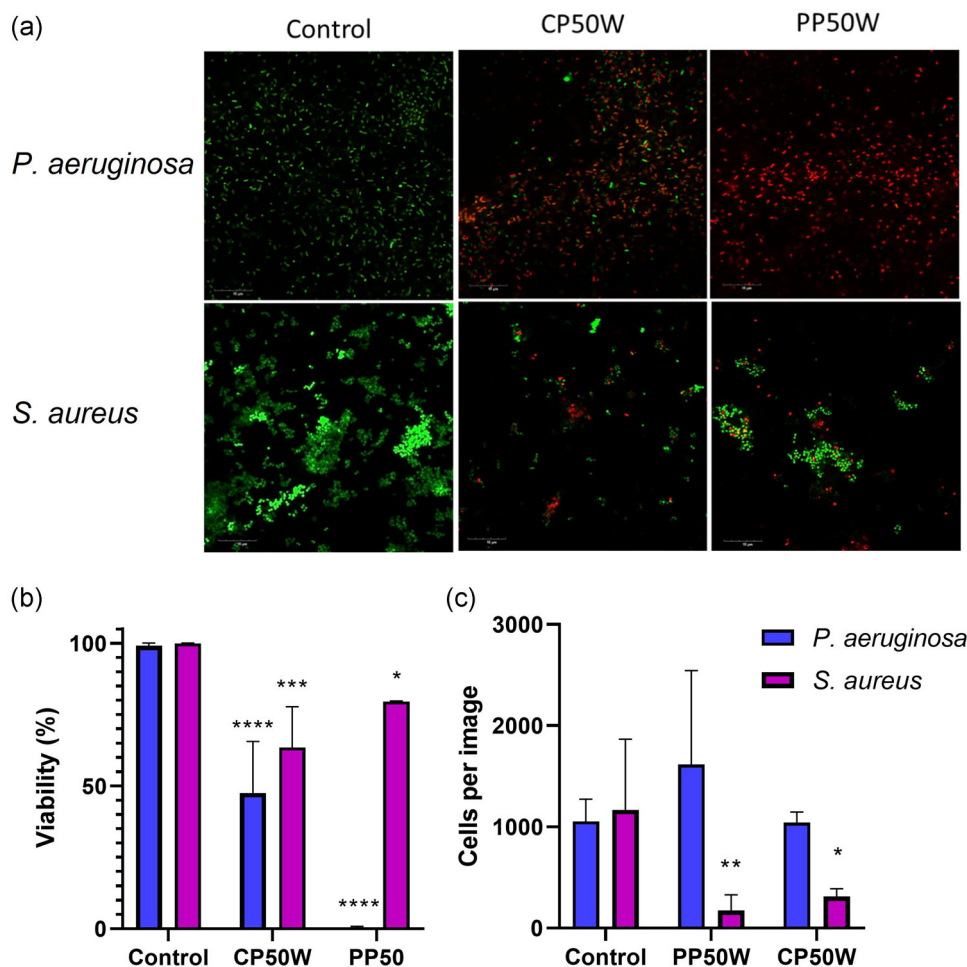

FIGURE 4 (a) Dynamic wetting properties of CP50W and PP50W over time (30 s) evaluated by sessile drop water contact angle measurements. (b) Photographs of water droplets on CP50W and PP50W

FIGURE 5 Antibacterial effect of plasma polymer (PP)-oregano secondary metabolites. (a) LIVE/DEAD images of *Pseudomonas aeruginosa* and *Staphylococcus aureus*. The green dye represents live bacteria, whereas the red stain represents dead bacteria. (b) Viability. (c) Cells per image. The dimensions of fluorescence images are approximately $100 \times 100\,\mu m$

immunofluorescence staining using vimentin (green) and DAPI (blue) (see Figure 6b). Vimentin is an intermediate filament that acts as a signaling mediator between cells by regulating cellular processes of relevance in wound healing, like adhesion, migration, differentiation, and morphological arrangements.[45,46] Figure 4 shows that fibroblasts adhered and spread well in all samples. Corrected total fluorescence was calculated using ImageJ software (Figure 6a, right panel). CP50W and PP50W were not cytotoxic and biocompatible with human dermal fibroblasts, which suggests their potential for use in devices that are in contact with dermal tissue.

One of the main features of the presented polymers was their antibacterial and antifouling properties, which are similar to the antibacterial behavior shown by PP from T4 and geranium monomers fabricated at low plasma power levels.[19,24,26] In addition to the antibacterial and antifouling study of oregano, this is the first study where fibroblasts' viability, cytotoxicity, and cell

adhesion were evaluated for PP-OSMs. Considering these data, our results suggest that PP-OSMs have potential use as coatings for different medical devices, for example, as a coating for dermal wound dressings, catheters, and implants. Nevertheless, in vivo assessments would be interesting to determine the optimal performance of PP-OSMs, especially when they are in contact with living tissue in a wound environment.

4 | CONCLUSION

Plasma polymer films from OSMs were successfully developed at different RF power levels using RF-PECVD. The functional groups of the oregano monomer were retained in the PP-OSMs, resulting in a smooth and hydrophilic polymer. The surface roughness of CP50W resulted in a hydrophilic surface, whereas PP50W had a contact angle of 5° and is, therefore, considered superhydrophilic. The results suggest that coating leachate of
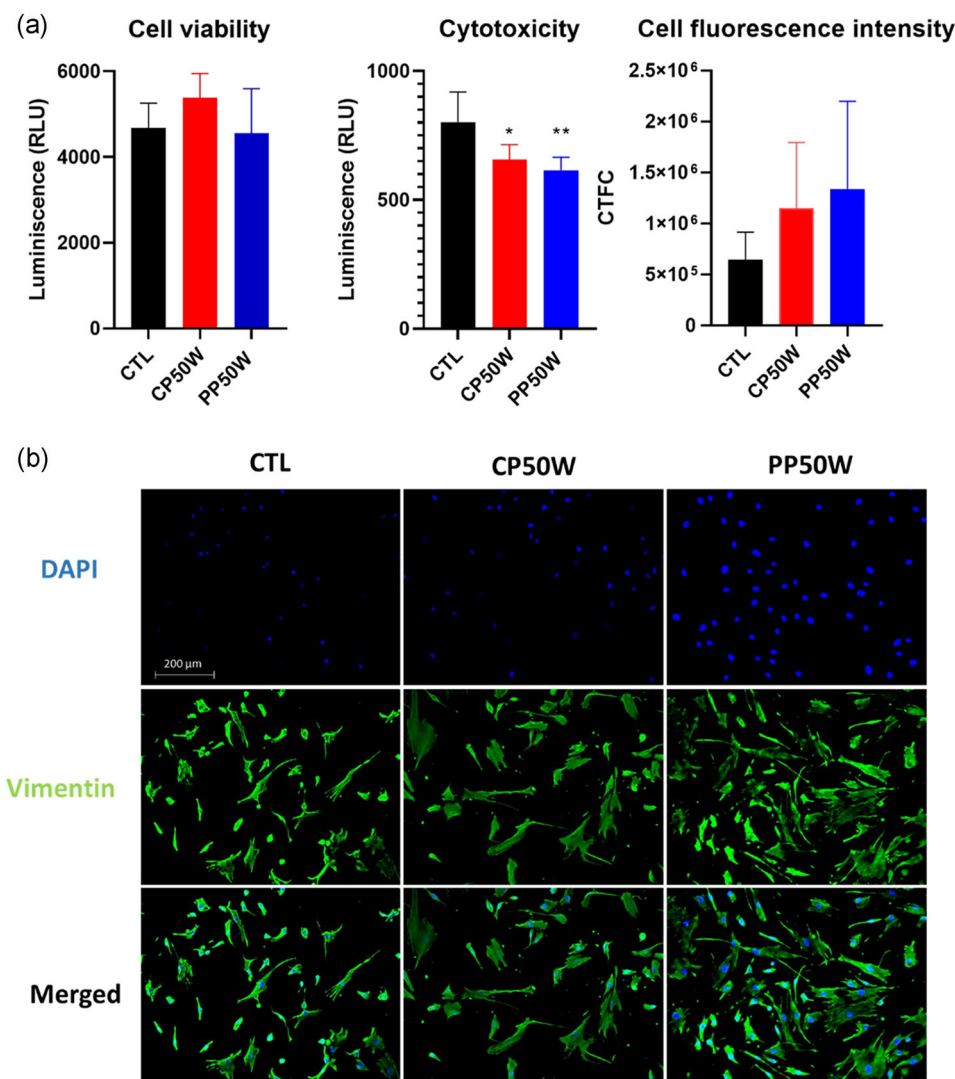
FIGURE 6 (a) Plots for viability, cytotoxicity, and fluorescence intensity of human dermal fibroblast after being seeded in plasma polymer (PP)-oregano secondary metabolites for 24 h. (b) Fluorescence images using 4′,6-diamidino-2-phenylindole as a nucleus staining (blue) and vimentin as a cytoskeleton filament staining (green)

the PP-OSMs modifies the pH of the media used. PP-OSMs was shown to have bactericidal properties against Gram-negative *P. aeruginosa* and antifouling properties against Gram-positive *S. aureus*. Moreover, PP-OSMs supported fibroblasts′ growth and proliferation without producing significant cytotoxicity. Adhesion and spread of fibroblasts on PP-OSMs were also confirmed. The overall results suggest the potential application of these polymers in medical applications, such as wound dressings, where antibacterial and biocompatibility are required.

CONFLICTS OF INTEREST

The authors declare no conflicts of interest.

DATA AVAILABILITY STATEMENT

Data are available on request from the authors.

ORCID

Jesus Romo-Rico https://orcid.org/0000-0002-3538-0539

Smriti Murali Krishna https://orcid.org/0000-0002-0810-5144

Mohan V. Jacob https://orcid.org/0000-0002-2598-7193

REFERENCES

[1] Z. Yao, J. Niu, B. Cheng, *Adv. Skin Wound Care* **2020**, *33*, 1.

[2] S. R. Nussbaum, M. J. Carter, C. E. Fife, J. DaVanzo, R. Haught, M. Nusgart, D. Cartwright, *Value Health* **2018**, *21*, 27.

[3] C. J. Phillips, I. Humphreys, J. Fletcher, K. Harding, G. Chamberlain, S. Macey, *Int. Wound J.* **2016**, *13*, 1193.

[4] H. Edwards, K. Finlayson, M. Courtney, N. Graves, M. Gibb, C. Parker, *BMC Health Serv. Res.* **2013**, *13*, 86.

[5] L. McCosker, R. Tulleners, Q. Cheng, S. Rohmer, T. Pacella, N. Graves, R. Pacella, *Int. Wound J.* **2019**, *16*, 84.

[6] J. J. van Netten, P. A. Lazzarini, R. Fitridge, E. Kinnear, I. Griffiths, M. Malone, B. Perrin, J. Prentice, S. Sethi, P. Wraight, *Australian Diabetes-Related Foot Disease Strategy 2018–2022: The First Step Towards Ending Avoidable Amputations within a Generation*, Diabetic Feet Australia, Wound Management CRC, Brisbane, Australia **2017**.

[7] S. Verbanic, Y. Shen, J. Lee, J. M. Deacon, I. A. Chen, *npj Biofilms Microbiomes* **2020**, *6*, 21.

[8] N. Misra, S. Bhatt, F. Arefi-Khonsari, V. Kumar, *Plasma Processes Polym.* **2021**, *18*, e2000215.

[9] Y. Ferreira da Silva, V. M. Queiroz, I. C. S. Kling, B. S. Archanjo, R. N. Oliveira, R. A. Simao, *Plasma Processes Polym.* **2020**, *17*, 2000035.

[10] M. Y. Huang, M. H. Liao, Y. K. Wang, Y. S. Huang, H. C. Wen, *Am. J. Chin. Med.* **2012**, *40*, 845.

[11] C. Cheng, Y. Zou, J. Peng, *Molecules* **2018**, *24*, 23.

[12] Z. W. Cui, Z. X. Xie, B. F. Wang, Z. H. Zhong, X. Y. Chen, Y. H. Sun, Q. F. Sun, G. Y. Yang, L. G. Bian, *Acta Pharmacol. Sin.* **2015**, *36*, 1426.

[13] M. N. Gallucci, M. E. Carezzano, M. M. Oliva, M. S. Demo, R. P. Pizzolitto, M. P. Zunino, J. A. Zygadlo, J. S. Dambolena, *J. Appl. Microbiol.* **2014**, *116*, 795.

[14] A. Puskarova, M. Buckova, L. Krakova, D. Pangallo, K. Kozics, *Sci. Rep.* **2017**, *7*, 8211.

[15] H. Y. Cui, C. H. Zhang, C. Z. Li, L. Lin, *Ind. Crops Prod.* **2019**, *139*, 103.

[16] D. Trombetta, F. Castelli, M. G. Sarpietro, V. Venuti, M. Cristani, C. Daniele, A. Saija, G. Mazzanti, G. Bisignano, *Antimicrob. Agents Chemother.* **2005**, *49*, 2474.

[17] R. J. W. Lambert, P. N. Skandamis, P. J. Coote, G. J. E. Nychas, *J. Appl. Microbiol.* **2001**, *91*, 453.

[18] A. Ultee, M. H. J. Bennik, R. Moezelaar, *Appl. Environ. Microbiol.* **2002**, *68*, 1561.

[19] O. Bazaka, K. Bazaka, V. K. Truong, I. Levchenko, M. V. Jacob, Y. Estrin, R. Lapovok, B. Chichkov, E. Fadeeva, P. Kingshott, R. J. Crawford, E. P. Ivanova, *Appl. Surf. Sci.* **2020**, *521*, 146375.

[20] K. Bazaka, M. V. Jacob, R. J. Crawford, E. P. Ivanova, *Acta Biomater.* **2011**, *7*, 2015.

[21] K. Bazaka, M. V. Jacob, *Mater. Lett.* **2009**, *63*, 1594.

[22] K. Bazaka, M. Jacob, V. K. Truong, R. J. Crawford, E. P. Ivanova, *Polymers* **2011**, *3*, 388.

[23] A. Kumar, A. Al-Jumaili, K. Prasad, K. Bazaka, P. Mulvey, J. Warner, M. V. Jacob, *Plasma Chem. Plasma Process.* **2019**, *40*, 339.

[24] A. Kumar, A. Al-Jumaili, K. Bazaka, P. Mulvey, J. Warner, M. V. Jacob, *Materials* **2020**, *13*, 586.

[25] A. Pegalajar-Jurado, C. D. Easton, K. E. Styan, S. L. McArthur, *J. Mater. Chem. B* **2014**, *2*, 4993.

[26] A. Al-Jumaili, K. Bazaka, M. V. Jacob, *Nanomaterials* **2017**, *7*, 270.

[27] R. Polat, F. Satil, *J. Ethnopharmacol.* **2012**, *139*, 626.

[28] J. Coccimiglio, M. Alipour, Z. H. Jiang, C. Gottardo, Z. Suntres, *Oxid. Med. Cell Longev.* **2016**, *2016*, 1404505.

[29] K. Malik, M. Ahmad, M. Zafar, R. Ullah, H. M. Mahmood, B. Parveen, N. Rashid, S. Sultana, S. N. Shah, Lubna, *BMC Complement. Altern. Med.* **2019**, *19*, 210.

[30] K. Singletary, *Nutrition Today* **2010**, *45*, 129.

[31] H. Yin, X. C. Fretté, L. P. Christensen, K. Grevsen, *J. Agric. Food Chem.* **2012**, *60*, 136.

[32] M. Bertuola, N. Fagali, M. Fernández, L. de Mele, *Heliyon* **2020**, *6*, e03714.

[33] S. Mediouni, J. A. Jablonski, S. Tsuda, A. Barsamian, C. Kessing, A. Richard, A. Biswas, F. Toledo, V. M. Andrade, Y. Even, M. Stevenson, T. Tellinghuisen, H. Choe, M. Cameron, T. D. Bannister, S. T. Valente, *J. Virol.* **2020**, 94.

[34] P.-Q. Gloria María, P.-Q. Gloria María, P.-Q. Gloria María, E.-R. Susana, C. Juan Pérez, A. María Rosa, A. María Rosa, V.-L. Blanca, V.-L. Blanca, *Front. Bioeng. Biotechnol.* **2021**, *9*, 703684.

[35] C. Watters, K. DeLeon, U. Trivedi, J. A. Griswold, M. Lyte, K. J. Hampel, M. J. Wargo, K. P. Rumbaugh, *Med. Microbiol. Immunol.* **2012**, *202*, 131.

[36] X. Xie, R. Zhong, L. Luo, X. Lin, L. Huang, S. Huang, L. Ni, B. Chen, R. Shen, L. Yan, C. Duan, *Immun. Inflamm. Dis.* **2021**, *9*, 1428.

[37] E. E. Johnston, B. D. Ratner, *J. Electron. Spectrosc. Relat. Phenom.* **1996**, *81*, 303.

[38] G. Schultz, D. Mozingo, M. Romanelli, K. Claxton, *Wound Repair Regen.* **2005**, *13*, S1.

[39] L. Watret, A. Rodgers, *Diabetic Foot* **2005**, *8*, 154.

[40] M. M. Gutiérrez-Pacheco, L. A. Ortega-Ramírez, B. A. Silva-Espinoza, M. R. Cruz-Valenzuela, G. A. González-Aguilar, J. Lizardi-Mendoza, R. Miranda, J. F. Ayala-Zavala, *Coatings* **2020**, *10*, 614.

[41] S. Beirão da Costa, C. Duarte, A. I. Bourbon, A. C. Pinheiro, A. T. Serra, M. Moldão Martins, M. I. Nunes Januário, A. A. Vicente, I. Delgadillo, C. Duarte, M. L. Beirão da Costa, *J. Food Eng.* **2012**, *110*, 190.

[42] X. Hui, G. Yan, F.-L. Tian, H. Li, W.-Y. Gao, *Med. Chem. Res.* **2017**, *26*, 442.

[43] S. Kumari, R. V. Kumaraswamy, R. C. Choudhary, S. S. Sharma, A. Pal, R. Raliya, P. Biswas, V. Saharan, *Sci. Rep.* **2018**, *8*, 6650.

[44] K.-Y. Law, *J. Phys. Chem. Lett.* **2014**, *5*, 686.

[45] C. De Pascalis, C. Pérez-González, S. Seetharaman, B. Boëda, B. Vianay, M. Burute, C. Leduc, N. Borghi, X. Trepat, S. Etienne-Manneville, *J. Cell. Biol.* **2018**, *217*, 3031.

[46] F. Cheng, Y. Shen, P. Mohanasundaram, M. Lindström, J. Ivaska, T. Ny, J. E. Eriksson, *Proc. Natl. Acad. Sci.* **2016**, *113*, E4320.

SUPPORTING INFORMATION

Additional supporting information can be found online in the Supporting Information section at the end of this article.